

Special Report

**PREDICTION OF THE POSITION OF AN ANIMAL BASED  
ON POPULATIONS OF GRID AND PLACE CELLS:  
A COMPARATIVE SIMULATION STUDY**

ALEXIS GUANELLA

*Institute of Neuroinformatics, University/ETH Zürich  
190 Winterthurerstrasse CH-8057 Zurich, Switzerland  
guanella@ini.phys.ethz.ch*

PAUL F. M. J. VERSCHURE

*ICREA & Technology Dept., University Pompeu Fabra  
Ocata 1, ES-08003 Barcelona, Spain  
paul.verschure@upf.edu*

Received 15 March 2007

Accepted 18 July 2007

The grid cells of the rodent medial entorhinal cortex (MEC) show activity patterns correlated with the animal's position. Unlike hippocampal place cells that are activated at only one specific location in the environment, MEC grid cells increase firing frequency at multiple regions in space, or subfields, that are arranged in regular triangular grids. It has been recently shown that a conjunction of MEC grid cells can lead to unique spatial representations. However, it remains unclear what the key properties of the grids are that allow for an accurate reconstruction of the position of the animal and what the comparison with hippocampal place cells is. Here we use a theoretical approach based on data from electrophysiological recordings of the MEC to simulate the neural activity of grid cells. Our simulations account for the accurate reproduction of grid cell mean firing rates, based on only three grid parameters, that is grid phase, spacing and orientation. The analysis of the key properties of the grids first reveals that for an accurate position reconstruction, it is necessary to combine cells with different grid spacings (which are found at different dorsoventral locations of the MEC) or orientations. Second, the relationship between grid spacing and subfield size observed in physiological data is optimal to predict the animal's position. Third, the regular triangular tessellating patterns of grid cells lead to the best position reconstruction results when compared with all other regular tessellations of two-dimensional space. Finally, the comparison of grid cells with place cells shows that populations of MEC grid cells can better predict the animal's position than equally-sized populations of hippocampal place cells with similar but unique spatial fields. Taken together, our results suggest that the MEC provides highly compact representations of the animal's position, which may be subsequently integrated by the place cells of the hippocampus.

*Keywords:* Grid cells; place cells; medial entorhinal cortex; hippocampus; position reconstruction; spatial cognition.

## 1. Introduction

A prerequisite for efficient navigation in complex environments is the ability to localize oneself in space. In mammals, neurons have been identified whose activity is correlated with the location of the animal. In particular, the place cells of the hippocampus are activated at specific and generally unique regions in an environment [1, 2]. It has been proposed that these neurons form a cognitive map, in which the location of the animal is represented [2–5]. Indeed, a population of hippocampal place cells provides highly specific position information that supports the accurate localization of a rat in an arena [6, 7]. More recently, the activity patterns of the so-called grid cells of the medial entorhinal cortex (MEC) were also found to correlate with the position of the animal [8–12]. One synapse upstream from the hippocampus, these cells increase firing frequency at multiple regions in an environment, or subfields, that are arranged in regular triangular grids. Neighboring grid cells share common grid spacing and orientation but different phases, and the grid spacing increases isometrically along the dorsoventral axis of the MEC, in a quadratically proportional relationship with the grid subfield size [10].

An individual grid cell expresses only ambiguous position information: the maximum firing rates of different subfields have similar intensities that are only weakly correlated over sessions [10]. It is thus difficult to discriminate between the multiple subfields, and, consequently, to determine the position of the animal when the cell is firing. It has been proposed that the integration of grids with different spacings and/or orientations could help to resolve this ambiguity [10]. Moreover, it has been recently shown that place cells can be mapped from grid cells [13–15] and that these place cells could provide unique place codes [16]. In the latter study [16], simulated grid cell activity patterns were used to drive a population of place cells. The correlation of the place cell population vector was then computed across different locations in the environment, in order to quantify the distinction between distant positions. This methodology allows to answering the question whether the animal's location can be uniquely determined from the population activity pattern of grid cells, but does not allow for a quantification and comparison of the relative contribution of grid cells with that of place cells. In addition, the use of a non-physiologically constrained model prevents the comparison with electrophysiological recordings.

Hence, in the present study, we quantify to what extent populations of grid cells can predict the position of an animal and use a physiologically constrained model that accurately reproduces the mean firing rates of grid cells combined with well established Bayesian position reconstruction method. To identify the different properties of the grids that allow for an accurate representation of the position of the animal, we first compare different subsets of neurons with distinct parameter distributions. Second, we generate populations of grid cells with different proportionality factors between grid spacing and subfield size, in order to determine whether the quadratic proportionality factor found in physiological data is optimal in terms of position reconstruction. Third, we make the comparison of the three

regular tessellations of two-dimensional space to determine which one provides the better quality position information. Finally, to compare the position information in populations of grid cells with populations of place cells, we construct equally-sized populations of place cells with similar, but unique subfields.

## 2. Methods

We use a theoretical approach to assess the question of the representation of the animal's position by a population of grid cells since, for several reasons, it is difficult to conduct these investigations experimentally. First, during a recording session, the grid cells of one hemisphere are generally recorded from a single location. According to the topographical organization of grid cells in the MEC, these neighboring cells share common grid spacing and orientation, and thus the same periodicity, which restricts the scope for integration over different grids. Second, it has not been possible so far to sample the activity of large enough numbers of cells in the MEC *in vivo*.

Our model simulates the activity of grid cells as a function of the position of a virtual rat exploring a  $1\text{ m} \times 1\text{ m}$  square arena. The grids are characterized by three parameters, the grid spacing  $d$ , orientation  $\alpha$  and phase  $\mathbf{p} = (p_x, p_y)$  (Fig. 1), that are uniformly distributed consistently with a previous study [10], i.e., the grid spacings are distributed between 0.39 m and 0.73 m, the grid orientations between  $0^\circ$  and  $60^\circ$  and the grid phases vary over the whole environment. The grid subfields are represented by a combination of Gaussian functions, whose centers regularly tessellate the environment with triangles. In addition, we integrate into the model the small random grid shifts and rotations across sessions, that can be observed in physiological data (Fig. 2 and Methods). We make as few assumptions as possible about how position information is generated in the MEC. Our model simply but accurately reproduces the firing rates of grid cells, with a mean squared residual error of less than 4% of the mean firing rates observed in physiological data (Fig. 2). Subsequently, we use a standard and well established Bayesian framework for position reconstruction [7] that is uniquely based on instantaneous neural firing rates and on the position of the animal.

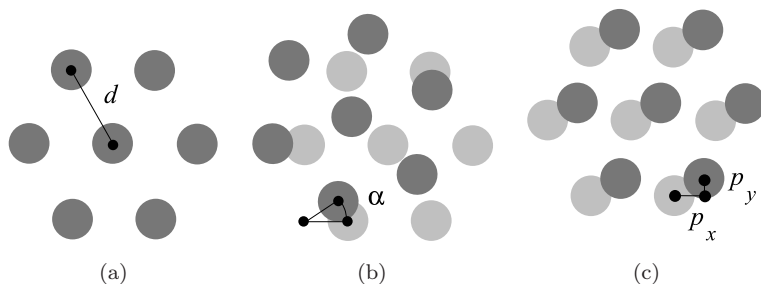


Fig. 1. Characterization of the grids with three parameters: (a) grid spacing  $d$ , (b) grid orientation  $\alpha$  and (c) grid phase  $\mathbf{p} = (p_x, p_y)$  (along the  $x$ - and  $y$ -axes). Circles represent grid subfields.

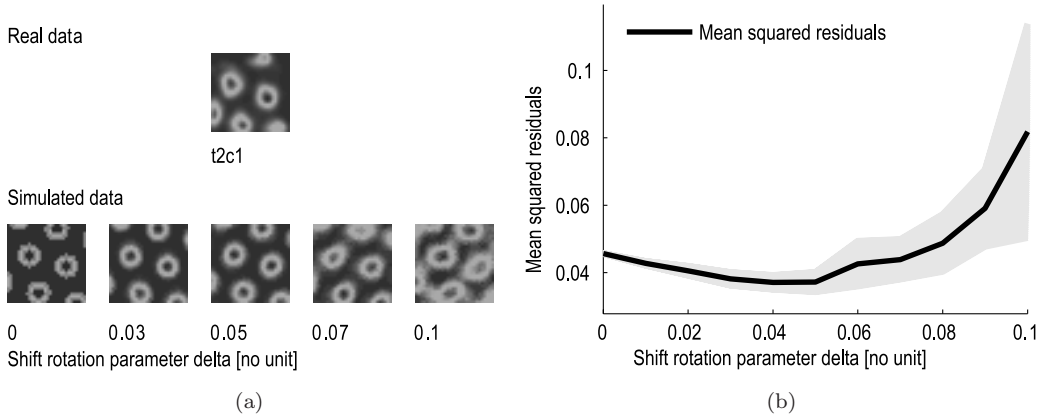


Fig. 2. Simulation of grid cells with small random grid shifts and rotations across trials. (a) *Top*: Mean activity map (i.e. mean activity of a cell as a function of the animal’s position in the arena, white = medium and black = low or high mean activity) of a real grid cell (recording time of 20 min). *Bottom*: Mean activity map of a simulated grid cell, whose grid parameters are fitted to the real cell, with different shift-rotation parameter values. (b) Mean squared residuals between real grid cell mean activity maps and simulated grid cell mean activity maps as a function of the shift-rotation parameter. The gray region indicates  $\pm$  s.d.

### 2.1. Generation of grid cell activity

The activity  $A(\mathbf{x})$  of a simulated grid cell is a function of the position  $\mathbf{x}$  of the animal:

$$A(\mathbf{x}) = \max_{k=1,2,3,4} \exp\left(-\frac{\|(\mathbf{R}_\alpha \mathbf{x} - \mathbf{p}) \bmod \mathbf{c} - \mathbf{s}_k\|^2}{\sigma^2}\right), \quad (1)$$

where the angle  $\alpha$  determines the grid orientation and where  $\mathbf{R}_\alpha$  is the rotation matrix defined by

$$\mathbf{R}_\alpha = \begin{pmatrix} \cos(\alpha) & \sin(\alpha) \\ -\sin(\alpha) & \cos(\alpha) \end{pmatrix}, \quad (2)$$

and where  $\mathbf{c} = (d, \sqrt{3}d)$ ,  $\mathbf{s}_1 = (d/2, 0)$ ,  $\mathbf{s}_2 = (0, \sqrt{3}d/2)$ ,  $\mathbf{s}_3 = (d, \sqrt{3}d/2)$ ,  $\mathbf{s}_4 = (d/2, \sqrt{3}d)$ .  $\sigma$  determines the subfield size and depends on  $d$ .

### 2.2. Generation of place cell activity

We compute place cell activity as a Gaussian function of two distal cues, representing two perpendicular walls in a square environment [17]. The place field size is determined by the parameter  $\tau$ , which has the same distribution as  $\sigma$ .

The equation of the activity  $B(\mathbf{x})$  of a place cell is thus given by

$$B(\mathbf{x}) = \exp\left(-\frac{\|\mathbf{x} - \mathbf{q}\|^2}{\tau^2}\right), \quad (3)$$

where  $\mathbf{q}$  is the position of the center of the place field. In our experiments,  $\mathbf{q}$  is uniformly distributed within the environment.

### 2.3. Small grid rotations and shifts across sessions

The place fields of hippocampal place cells are found to be slightly shifted across sessions [18]. Shifts of similar magnitude can be found in grid cell recordings, as well as small rotations of the grids (mean shifts of 4.2 cm along the x-axis of the grid, of 4.4 cm along the y-axis of the grid, and mean rotations of  $2.6^\circ$ , observed in a set of eight grid cells recorded in the dorsolateral band of the MEC (layer II), (data courtesy of the Center for Biology of Memory, NTNU, Norway [9]). To illustrate the robust readout of position in the grid cell activity, we integrate these small shifts and rotations in our model. Hence, the activity  $\tilde{A}(\mathbf{x})$  of a simulated grid cell with a small grid rotation  $\Delta\alpha$  and shift  $\Delta\mathbf{x}$  is

$$\tilde{A}(\mathbf{x}) = A(\mathbf{R}_{\Delta\alpha}(\mathbf{x} + \tilde{\mathbf{x}}) - \tilde{\mathbf{x}} + \Delta\mathbf{x}), \quad (4)$$

where  $\tilde{\mathbf{x}} \sim \mathcal{U}(0, 1) \times \mathcal{U}(0, 1)$  determines the center of the rotation of the grid and where  $\Delta\mathbf{x} \sim \mathcal{N}(0, \delta_x^2) \times \mathcal{N}(0, \delta_y^2)$  and  $\Delta\alpha \sim \mathcal{N}(0, \delta_\alpha^2)$ .  $\mathcal{U}(a, b)$  describes a uniform distribution between  $a$  and  $b$  and  $\mathcal{N}(\mu, \sigma^2)$  describes a normal distribution of mean  $\mu$  and variance  $\sigma^2$ . In our experiments, since  $\delta_x$ ,  $\delta_y$  and  $\delta_\alpha$  represent subfield motions of similar magnitude, we use  $\delta = \delta_x = \delta_y = \delta_\alpha$ .

### 2.4. Bayesian position reconstruction error

Given the activity  $\mathbf{n}(t)$  of a set of  $N$  cells at time  $t$ , i.e.  $\mathbf{n}(t) = (n_1(t), \dots, n_N(t))$ , we determine the reconstructed position  $\hat{\mathbf{x}}(t)$ , as the position  $\mathbf{x}(t)$  that maximizes the probability  $P(\mathbf{x}(t) | \mathbf{n}(t))$ . To compute the probabilities  $P(n_i(t) | \mathbf{x}(t)) \forall i = 1, \dots, N$ , derived from  $P(\mathbf{x}(t) | \mathbf{n}(t))$  using Bayes rule (Eq. (5)) [7], we discretize the environment into  $30 \times 30$  bins over  $1 \text{ m}^2$  and the cell activities into five activity levels. The choice of the activity discretization is justified by the observation that no critical improvement of the position reconstruction is found in a set of 16 cells with twice the resolution. We assume, without loss of generality, that the animal's trajectory covers the environment uniformly: we simulate 30 sessions in each of which each bin is visited exactly once. The probabilities are computed over a set of 29 sessions, the last session (so-called testing set) being used to compute the reconstructed position, given by

$$\hat{\mathbf{x}}(t) = \arg \max_{\mathbf{x}(t)} P(\mathbf{x}(t) | \mathbf{n}(t)) = \arg \max_{\mathbf{x}(t)} \prod_{i=1}^N P(n_i(t) | \mathbf{x}(t)) P(\mathbf{x}(t)). \quad (5)$$

### 2.5. Relationship between subfield size and grid spacing

The proportionality factor  $\beta$  describes the relationship — found in physiological recordings [10] — between the grid spacing  $d$  and  $\sigma$  (which determines the subfield size), and is computed as follows. To identify  $\beta$ , we define  $f$  as the size of the contiguous region where the firing rate is above 20% of the peak firing rate of the cell [9]. From [10], we have

$$d \times 0.55 = \sqrt{f}. \quad (6)$$

Assuming that the subfields of real grid cells have a circular shape and defining  $x$  as the subfield radius, we get

$$x = \sqrt{\frac{f}{\pi}} = \frac{d \times 0.55}{\sqrt{\pi}}. \quad (7)$$

Using the definition of a subfield and the definition of  $f$ , we get

$$e^{-(x/\sigma)^2} = 0.2, \quad (8)$$

or

$$x = \sqrt{-\ln 0.2} \sigma. \quad (9)$$

Thus,

$$\sigma = \frac{d \times 0.55}{\sqrt{-\pi \ln 0.2}}, \quad (10)$$

and

$$\beta = \frac{0.55}{\sqrt{-\pi \ln 0.2}} \simeq 0.25. \quad (11)$$

## 2.6. Computation of the chance level of the position reconstruction error

The chance level of the position reconstruction error can be computed as the mean distance  $E$  between two uniform random variables in a normalized square:

$$E = \sum_{i,j,k,l=0}^{M-1} \frac{\sqrt{(i-j)^2 + (k-l)^2}}{M^5}, \quad (12)$$

where  $M$  is the number of bins on a side. For  $M = 30$ , corresponding to the number of bins in this study, we have  $E \simeq 0.52$ . This value provides the theoretical chance level for the position reconstruction error that we get with the Bayesian method applied on grid and place cells.

## 2.7. Statistics

To determine whether the correlation coefficients of the peak subfield activity in short sessions of three minutes are different from zero in physiological recordings, we use a signed rank test, which assumes a symmetrical distribution. This assumption is assessed by a Kolmogorov-Smirnov test on the data, indicating no critical difference in the two-tailed distributions. In this study, statistical significance is set at a level of  $p < 0.05$ .

## 3. Results

### 3.1. Model validation

To determine the accuracy of our model to reproduce grid cell mean firing rates, we first computed the least square residuals of the mean activity maps of simulated

grid cells fitted to the mean activity maps of real grid cells (data courtesy of the Center for Biology of Memory, NTNU, Norway [9]), optimizing grid phase, spacing and orientation parameters. Small shifts and rotations of the grids using the shift-rotation parameter of  $\delta = 0.04$  (which corresponds to the value observed in physiological data, see Methods), minimized the mean squared residual difference between both maps (mean squared residuals of  $0.037 \pm 0.008$ , Fig. 2). In addition, the mean activity maps of the simulated grid cells were all significantly correlated to the mean activity maps of the real grid cells ( $p < 0.05$ ,  $t$ -test with  $30 \times 30^{-2}$  degrees of freedom).

To determine whether it was reasonable to model each subfield with similar intensity, we computed the correlation across sessions of the grid subfield peak firing rates of eight grid cells recorded in layer II of the dorsolateral band of the MEC. We used recording sessions of 3 min each in order to determine whether small differences in firing rates could be found repetitively in recording sessions whose size corresponds to the size of our testing sets. The distribution of the correlation coefficients was not significantly different from zero ( $r = 0.15 \pm 0.51$ , Wilcoxon signed rank test,  $p = 0.07$ , Fig. 3), indicating that it is not necessary to consider grid cells with different subfield peak firing rates.

### 3.2. Key properties of the grids that allow for an accurate position reconstruction

To assess the position information provided by a population of medial entorhinal grid cells, we generated the neural activity of grid cells with different grid spacings, orientations and phases [Figs. 1, 4(a) and 4(c)]. We computed the mean Euclidean

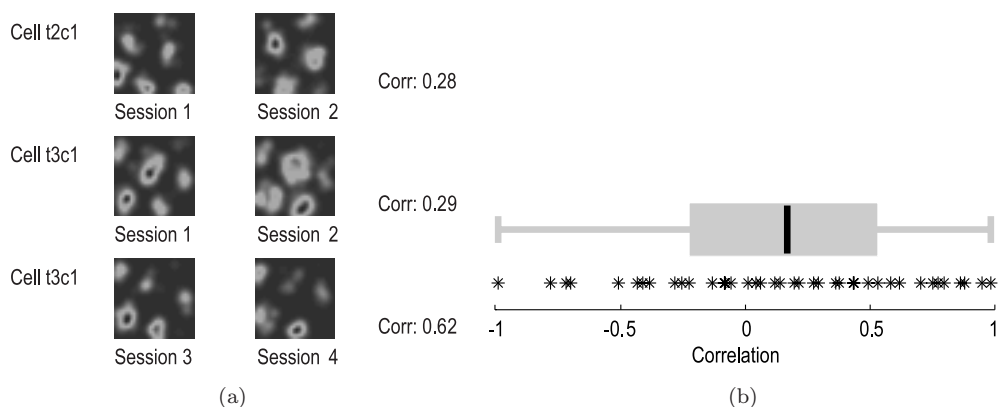


Fig. 3. Correlation of the grid subfield maximum activities across recording sessions. (a) Representative mean activity maps of three real grid cells of the dorsolateral band of the MEC (layer II), as a rat explores a  $1 \times 1$  square meter arena (rows 1 to 3). Cell names refer to tetrode ( $t$ ) and cell ( $c$ ) numbers. Correlation coefficients are indicated at the end of each row. (b) Correlation coefficient distribution. Each star represents the correlation coefficient of an individual cell between two recording sessions. The box plot indicates the median (dark line) and the inter-quartile range of the correlation coefficients (gray rectangle). Whiskers indicate the extent of the rest of the data.

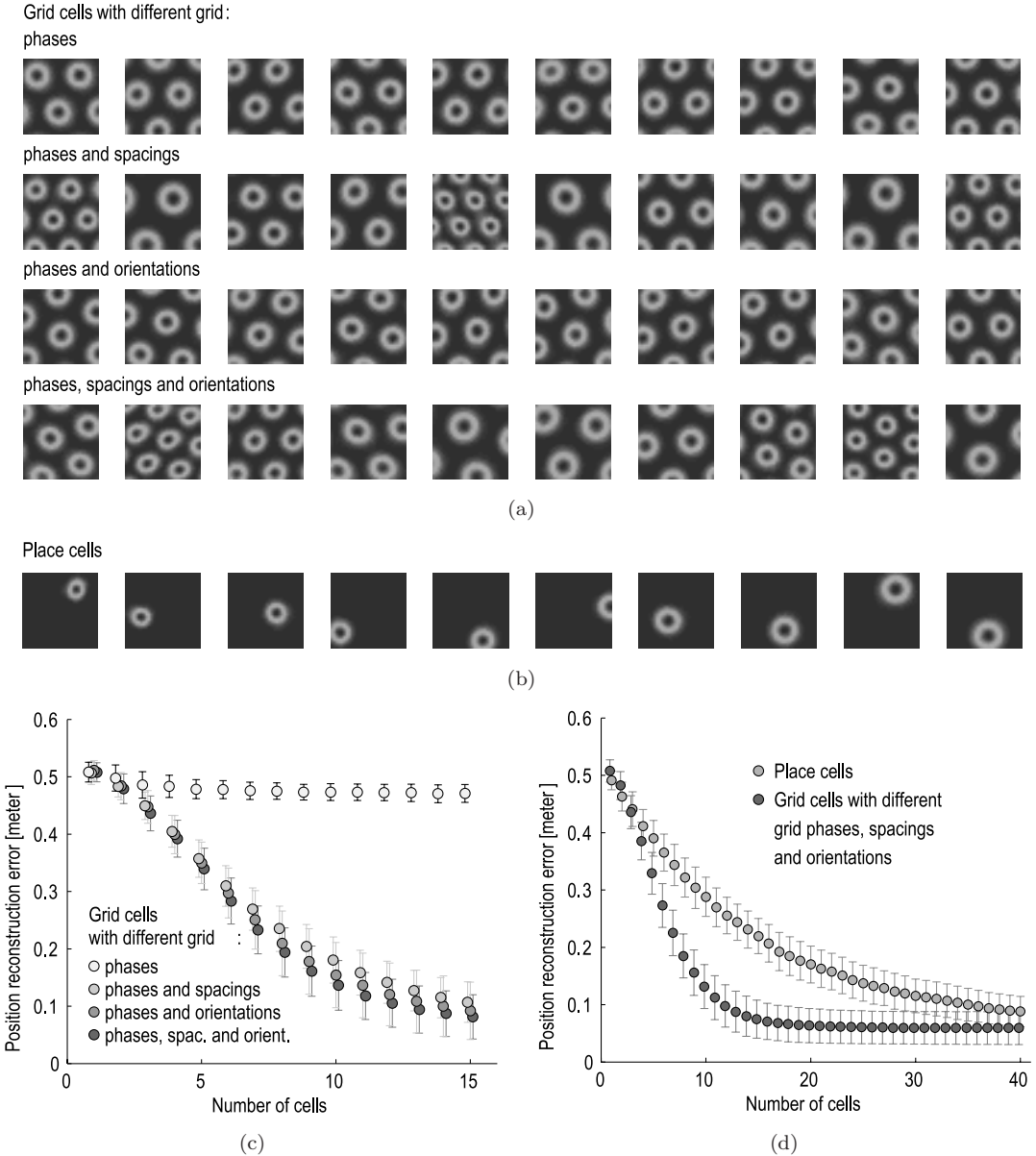


Fig. 4. Mean activity maps and position reconstruction error of simulated grid and place cells. (a) First row: mean activity maps of ten simulated grid cells with different grid phases. Second row: mean activity maps of ten simulated grid cells with different grid phases and spacings. Third row: mean activity maps of ten simulated grid cells with different grid phases and orientations. Fourth row: mean activity maps of ten simulated grid cells with different grid phases, spacings and orientations. (b) Mean activity maps of ten simulated place cells, sorted by place field size. (c) Comparison of the position reconstruction error of four different subsets of simulated grid cells: grid cells with different grid phases, with different grid phases and spacings, with different grid phases and orientations and with different grid phases, spacings and orientations. Error bars indicate  $\pm$  s.d. (d) Comparison of the position reconstruction error of a set of simulated grid cells with different grid phases, spacings and orientations with a set of simulated place cells, as a function of the number of cells.

distance between the simulated and the reconstructed position of the virtual rat (the so-called position reconstruction error, see Methods). For one grid cell, the position reconstruction error was of  $0.509 \text{ m} \pm 0.017 \text{ m}$  [mean  $\pm$  s.d., Fig. 4(c)], which is near the theoretical chance level of  $0.52 \text{ m}$  (Methods). The position reconstruction error rapidly decreased with an increase in the number of cells, reaching a plateau of  $0.06 \text{ m} \pm 0.03 \text{ m}$  for 25 cells and more. According to the topographical organization of grid cells in the MEC, we constructed three additional subsets of neurons. The first subset was composed of neighboring cells, sharing the same grid spacing and orientation, but with different grid phases. The second subset was composed of non-neighboring cells at the same dorsoventral location, sharing the same grid spacing, but with different grid phases and orientations, and the third subset was composed of cells along the dorsoventral axis of the MEC sharing the same grid orientation, but with different grid phases and spacings. We observed that the subset of neighboring grid cells did not provide high position information, i.e. the position reconstruction error was of  $0.468 \text{ m} \pm 0.017 \text{ m}$  for 15 cells, near the theoretical chance level [Fig. 4(c), Methods]. This high error is explained by the impossibility of disambiguating between different repetitive grid patterns among cells in a population where only grid translations occur. The superposition of these repetitive patterns with identical periodicity leads to a population that shares the same ambiguity problem as an individual cell. With varying spacings and/or orientations in the subsets of grid cells, the position reconstruction errors were drastically reduced [Fig. 4(c), provided by populations of 15 cells]: position reconstruction errors of  $0.107 \text{ m} \pm 0.050 \text{ m}$  with varying phases and spacings, of  $0.092 \text{ m} \pm 0.039 \text{ m}$  with varying phases and orientations (in this case, grid spacing was fixed at  $56 \text{ cm}$ , that is exactly between  $39 \text{ cm}$  and  $73 \text{ cm}$ ) and of  $0.081 \text{ m} \pm 0.036 \text{ m}$  with varying phases, spacings and orientations. The minimum position reconstruction error was achieved in the population of grid cells where different grid spacings, orientations, and phases were combined.

### 3.3. Proportion between grid spacing and subfield size

To determine whether the proportion between grid spacing and subfield size observed in physiological data was optimal in terms of position reconstruction error, we constructed grid cell populations with different proportionality factors (Methods and Fig. 5). We observed no critical difference between the minimal position reconstruction error ( $0.053 \text{ m} \pm 0.027 \text{ m}$ , using populations of 25 cells and corresponding to a value of beta of 0.4) and the position reconstruction error using the proportionality factor of 0.25 found in physiological recordings (Fig. 5, position reconstruction error of  $0.06 \text{ m} \pm 0.03 \text{ m}$ ).

### 3.4. Triangular structure of the grids

To determine the role of the regular triangular structure of grid cells, and, in particular, to determine whether triangular patterns lead to a minimal position

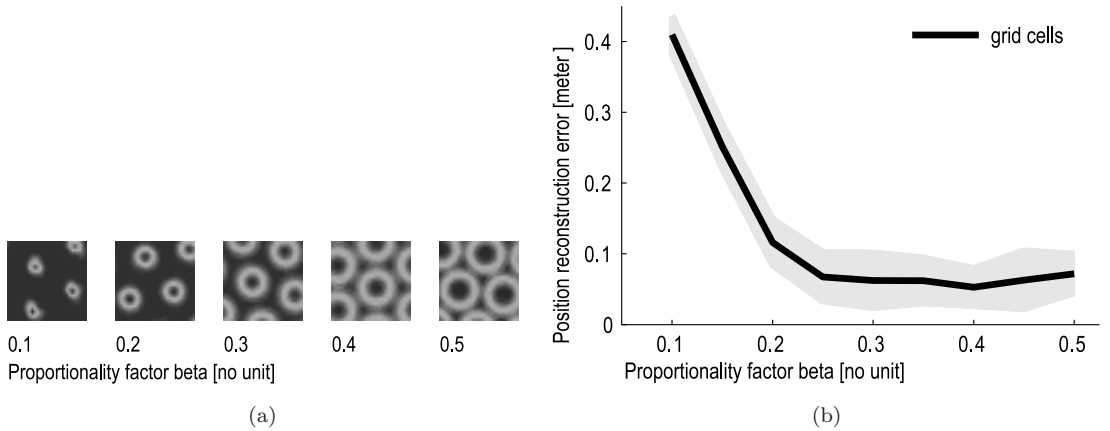


Fig. 5. Position reconstruction error as a function of the grid subfield size. (a) Mean activity maps of simulated grid cells with different values of  $\beta$ , describing the proportional relationship between grid spacing and the square root of the grid subfield size (Methods). (b) Position reconstruction error of a population of 15 simulated grid cells as a function of the parameter  $\beta$ . The gray region indicates  $\pm$  s.d.

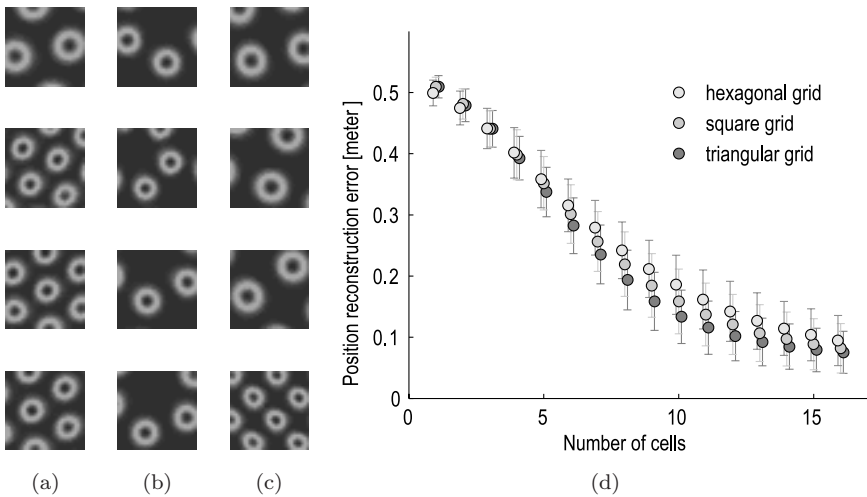


Fig. 6. Comparison of the position reconstruction error of grid cells with different regular tessellating patterns. (a) Mean activity maps of four simulated (triangular) grid cells. (b) Mean activity maps of four simulated hexagonal grid cells. (c) Mean activity maps of four simulated square grid cells. (d) Position reconstruction error of simulated triangular, hexagonal and square grid cells, as a function of the number of cells. Error bars indicate  $\pm$  s.d.

reconstruction error, we compared regular triangular tessellations with the other two regular tessellations of two-dimensional space, i.e. square and hexagonal regular tessellations. We observed that the position reconstruction error of grid cells with square and hexagonal grids was higher than the position reconstruction error of grid cells with triangular grids (Fig. 6). This shows that the triangular grid structure provides an optimal encoding of location in small populations of grid cells, which

is theoretically explained by the observation that a regular triangular tessellation represents the densest of all possible circle packings [19].

### 3.5. Comparison between grid and place cells

In order to compare the position information provided by entorhinal grid cells with that generated by hippocampal place cells, we created populations of place cells based on a well established model [17], with equivalent but unique subfields (Methods). We observed that the position reconstruction error of sets of four to 40 grid cells was critically smaller than that found in equally-sized sets of place cells with similar subfields [Fig. 4(d)]. In larger populations, no critical difference was observed between grid and place cells. It is interesting to note that the position reconstruction error of individual cells was smaller in place cells ( $0.489 \text{ m} \pm 0.017 \text{ m}$ ) than in grid cells ( $0.509 \text{ m} \pm 0.017 \text{ m}$ ). This illustrates the ambiguity of the representation of location provided by individual grid cells.

## 4. Discussion

Using a physiologically constrained model that accurately reproduces the activity patterns of entorhinal grid cells, we have quantified to what extent populations of entorhinal grid cells can predict the position of an animal and analyzed what the key properties of grid cells are that allow for an accurate position reconstruction. In addition, we have compared the positional information provided by populations of grid and place cells.

The comparison of different subsets of grid cells with distinct grid parameter distributions allows us to determine whether a combination of cells from the whole MEC is necessary for the read-out of the location of the animal by place cells. We observed that a combination of grid cells at the same dorsoventral region (with different orientations) is sufficient to allow for an accurate position reconstruction, suggesting that the combination of cells of the whole MEC is not required. The connections between the MEC and the hippocampus have been shown to be topographically organized from the dorsolateral to ventromedial axis in MEC to the dorsal to ventral (or septotemporal) axis of the hippocampus [9, 20, 21]. Our results thus suggest that combinations of different orientations found at the same dorsoventral region in the MEC are primarily used to extract location information and facilitate the formation of place cells.

To determine whether grid cells could represent the position of the animal within much bigger environments, it is interesting to consider the topographical organization of grid cells along the dorsoventral axis of the MEC. In fact, a simple pre-defined mechanism to form place cells from grid cells has been proposed [22] and implemented [13], where grid cells with peak firing rates at a given location are connected to the place cells whose place fields are centered at that location. This association mechanism explains why place fields increase in size when moving along the dorsoventral axis of the hippocampus [23]. Small place fields (and consequently

dense grids) might be used to represent the animal's position in small environments, whereas larger place fields might be used in larger environments. Unfortunately, the exact range of different grid spacings in the MEC is still not yet clearly defined, since grid cells have been so far only recorded in the most dorsal region of the MEC [10–12]. However, a recent finding could be used to identify it easily. Indeed, simple experiments report a correlation between grid spacings and subthreshold oscillations of stellate cells of the MEC [24]. Thus, it may be possible to estimate this range *in vitro* and therefore estimate to what extent grid cells might represent position within much larger environments.

Our model provides a straightforward mathematization of grid cells and allows for a high level modeling of their firing activity. Importantly, one of its convenient aspects is based on the assumption that no consistent pattern is present in the different peak firing rates at different grid nodes, which was assessed in this study using neurophysiological data (Results and Fig. 3). The question remains however open, whether specific experimental conditions could influence the peak firing rates of certain subfields across sessions. To test this hypothesis, additional investigations would be needed.

By showing that populations of MEC grid cells can better predict the position of an animal than equally-sized populations of hippocampal place cells in addition to the conjunctive representations of the heading direction and the running speed of the rat [11], our results suggest that the MEC implements highly compact distributed representations of spatial information. This is further validated by the optimality in terms of position reconstruction of the quadratic proportionality between subfield size and grid spacing observed in physiological data [10], and by the observation that the regular triangular patterns of grid cells generate the most compact representation of position, when compared with the other regular tessellating patterns of two-dimensional space. Such a compact coding might be justified by economy in wiring and the number of cells, and further research is necessary to determine how this spatial information might be subsequently integrated by other structures in the brain. In particular, although the position representation in populations of grid cells is compact and accurate, it is certainly not represented in a way that facilitates associations with other sources of information. It has been shown that the spatial information of the MEC is fundamentally dissociated from non-spatial information in the lateral entorhinal cortex [25], which indicates that these two input pathways can only be associated downstream in the hippocampus. This suggests that the compact spatial representations of the MEC are subsequently integrated by the place cells of the hippocampus to provide an associative substrate that allows for specific information to be correlated with single locations and individual cells [18].

## Acknowledgments

The authors thank Torkel Hafting and Marianne Fyhn for providing data from the MEC and for comments on this study, and Kynan Eng and Armin Duff for their

feedback on the manuscript. This research was supported by the Swiss National Science Foundation (grant nr. 205321-100604 to P.V.).

## References

- [1] O'Keefe J, Dostrovsky J, The hippocampus as a spatial map. Preliminary evidence from unit activity in the freely-moving rat, *Brain Res* **34**(1):171–175, 1971.
- [2] O'Keefe J, Nadel L, *The Hippocampus as a Cognitive Map*, Clarendon Press, Oxford, 1978.
- [3] Tolman E, Cognitive maps in rats and men, *Psych Rev* **55**(4):189–208, 1948.
- [4] Redish A, Touretzky D, Cognitive maps beyond the hippocampus, *Hippocampus* **7**(1):15–35, 1997.
- [5] Redish AD, *Beyond the Cognitive Map. From Place Cells to Episodic Memory*, The MIT Press, Cambridge, Massachusetts, 1999.
- [6] Wilson M, McNaughton B, Dynamics of the hippocampal ensemble code for space, *Science* **261**(5124):1055–1058, 1993.
- [7] Zhang K, Ginzburg I, McNaughton B, Sejnowski T, Interpreting neuronal population activity by reconstruction: Unified framework with application to hippocampal place cells, *J Neurophysiol* **79**(2):1017–1044, 1998.
- [8] Quirk G, Muller R, Kubie J, Ranck J, The positional firing properties of medial entorhinal neurons: Description and comparison with hippocampal place cells, *J Neurosci* **12**(5):1945–1963, 1992.
- [9] Fyhn M, Molden S, Witter MP, Moser EI, Moser MB, Spatial representation in the entorhinal cortex, *Science* **305**(5688):1258–1264, 2004.
- [10] Hafting T, Fyhn M, Molden S, Moser MB, Moser EI, Microstructure of a spatial map in the entorhinal cortex, *Nature* **436**(7052):801–806, 2005.
- [11] Sargolini F, Fyhn M, Hafting T, McNaughton BL, Witter MP, Moser MB, Moser EI, Conjunctive representation of position, direction, and velocity in entorhinal cortex, *Science* **312**(5774):758–762, 2006.
- [12] Fyhn M, Hafting T, Treves A, Moser MB, Moser EI, Hippocampal remapping and grid realignment in entorhinal cortex, *Nature* **446**(7132):190–194, 2007.
- [13] Solstad T, Moser EI, Einevoll GT, From grid cells to place cells: A mathematical model, *Hippocampus* **16**(12):1026–1031, 2006.
- [14] McNaughton BL, Battaglia FP, Jensen O, Moser EI, Moser MB, Path integration and the neural basis of the “cognitive map”, *Nat Rev Neurosci* **7**(8):663–678, 2006.
- [15] Rolls ET, Stringer SM, Elliot T, Entorhinal cortex grid cells can map to hippocampal place cells by competitive learning, *Network* **17**(4):447–465, 2006.
- [16] Fuhs MC, Touretzky DS, A spin glass model of path integration in rat medial entorhinal cortex, *J Neurosci* **26**(16):4266–4276, 2006.
- [17] O'Keefe J, Burgess N, Geometric determinants of the place fields of hippocampal neurons, *Nature* **381**(6581):425–428, 1996.
- [18] Leutgeb S, Leutgeb JK, Barnes CA, Moser EI, McNaughton BL, Moser MB, Independent codes for spatial and episodic memory in hippocampal neuronal ensembles, *Science* **309**(5734):619–623, 2005.
- [19] Steinhaus H, *Mathematical Snapshots*, 3rd edn, Dover, 1999.

- [20] Dolorfo C, Amaral D, Entorhinal cortex of the rat: Organization of intrinsic connections, *J Comp Neurol* **398**(1):49–82, 1998.
- [21] Witter M, Wouterlood F, Naber P, Haefliger TV, Anatomical organization of the parahippocampal-hippocampal network, *Ann NY Acad Sci* **911**:1–24, 2000.
- [22] O’Keefe J, Burgess N, Dual phase and rate coding in hippocampal place cells: Theoretical significance and relationship to entorhinal grid cells, *Hippocampus* **15**(7):853–866, 2005.
- [23] Maurer AP, Vanhoads SR, Sutherland GR, Lipa P, McNaughton BL, Self-motion and the origin of differential spatial scaling along the septo-temporal axis of the hippocampus, *Hippocampus* **15**(7):841–852, 2005.
- [24] Giocomo LM, Zilli EA, Hasselmo ME, Differences in subthreshold oscillations of stellate cells map to differences in periodicity of grid cells, *COSYNE 2007 Abstracts* **2**:80, 2007.
- [25] Hargreaves EL, Rao G, Lee I, Knierim JJ, Major dissociation between medial and lateral entorhinal input to dorsal hippocampus, *Science* **308**(5729):1792–1794, 2005.